

# Bachelor Thesis

## Finding an Optimal Regularisation Parameter for the Inversion of Transient Electromagnetic Data Using the L-Curve Method

Peter Balogh

e12202337@student.tuwien.ac.at

Matr.Nr. 1220 2337

Date: November 15, 2025

Supervisor: Associate Prof. Dr.rer.nat. Adrian Flores-Orozco

### Abstract

## 1 Introduction

## 2 Materials and Methods

The TEM method was originally introduced for mining applications (Chandra 2016) and was since adopted to other fields like groundwater, and geothermal exploration (Chandra 2016; Everett 2013). The transient electromagnetic (TEM) or alternatively time-domain electromagnetic (TDEM) method was proposed by Obukhov (1968) and has been intensively developed in the 1980s (Christiansen et al. 2006).

### 2.1 Transient Electromagnetic Method

For the TEM method a pulse of current is transmitted through a ungrounded transmitter loop generating a primary magnetic field (Chandra 2016; Christiansen et al. 2006). When the current is turned off, the decay of the primary field induces secondary currents (eddy currents) in the ground, which produce a secondary magnetic field (Chandra 2016; Christiansen et al. 2006). This is governed by the Maxwell equations, which state that a changing electrical field

induces a magnetic field, and vice versa (Christiansen et al. 2006). An electromagnetic (EM) wave propagating through the subsurface, is attenuated by the electrical properties of the materials it encounters (Christiansen et al. 2006; Everett 2013). The strength of the secondary magnetic field depends on the conductivity of the material the EM wave propagates through and by measuring this field over time using a receiver loop, information about the subsurface can be obtained (Christiansen et al. 2006; Chandra 2016). Data is recorded in specific time-windows (gates), which are usually logarithmically spaced to increase signal-to-noise (S/N) ratio in later times, which is called logging (Christiansen et al. 2006). Such a decay curve of the secondary magnetic field over time is called a “transient”, with an numerically modelled example shown in Figure 1(b).

By analysing the decay characteristics of a transient, it is possible to infer the conductivity structure of the subsurface, because with passing time the EM wave propagates deeper into the subsurface and thus later time gates are linked to information about deeper layers (Christiansen et al. 2006). The depth of investigation

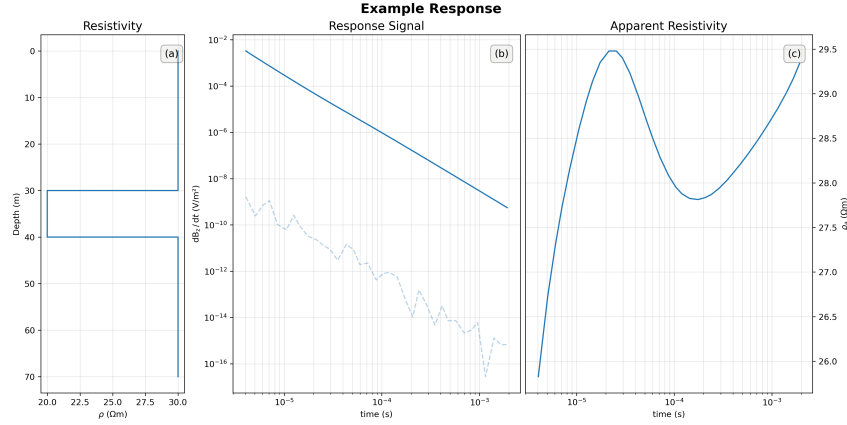


**Fig. 1:** Numerically modelled typical TEM response with the used subsurface model (a), the signal (b), and the apparent resistivity (c).

(DOI) is limited by the electrical conductivity of the subsurface, because a EM wave attenuates stronger within a conductive layer (Everett 2013). For this reason the TEM method is commonly deployed to investigate conductive layers such as sea water intrusions, and clay layers confining aquifers (Chandra 2016).

Every geophysical measurement includes uncertainty and a single transient is usually significantly influenced by background noise (Christiansen et al. 2006; Everett 2013). To increase the S/N ratio of a TEM sounding measurements are repeated and the resulting transients are combined, which is called “stacking” (Christiansen et al. 2006). Commonly between 1000 and 10000 transients are stacked into one sounding (Aigner et al. 2021) and when utilising a log-gating technique the S/N ratio is improved by the factor  $\sqrt{N}$  where N is the amount of measurements per stack (Christiansen et al. 2006).

A first evaluation of the data collected can be to convert the transient from voltage readings to apparent electrical resistivity ( $\rho_a$ ), which equals to the weighted mean of the resistivities of the layers in which the currents were induced (Siemon 2009). If the EM wave travels through a half-space, the late-time apparent resistivities is given by

$$\rho_a = \frac{1}{\pi} \left( \frac{M}{20 \cdot \frac{\partial b_z}{\partial t}} \right)^{\frac{2}{3}} \left( \frac{\mu_0}{t} \right)^{\frac{5}{3}} \quad (1)$$

where  $M$  is the magnetic moment,  $\frac{\partial b_z}{\partial t}$  is the signal measured by the receiver coil,  $\mu_0$  is the magnetic permeability of free space and  $t$  is

the time (Fitterman et al. 1986). The magnetic moment is the product of the number of turns, the area, and the current in the transmitter loop. Figure 1 shows a numerically modelled example, where (a) is the one dimensional model of the layered half-space, (b) is the modelled decay of the secondary magnetic field, and (c) shows the converted apparent resistivity. Figure 1 shows that in a layered half-space the resistivities of the subsurface model in (a) can not be simply inferred through the apparent resistivities in (c), which makes the interpretation of the data necessary (Fitterman et al. 1986; Christiansen et al. 2006). Reconstructing the resistivity distribution of the subsurface requires the solution of ill-posed problem, as there are many subsurface models, which can explain the measured data (Xue et al. 2020). Inferring a subsurface model from observed data is called an inverse problem or “inversion” and will be discussed in section 2.2.3. For the interpretation of TEM data – and for the inversion in particular – the following assumptions must to be made: The EM waves created by the transmitter only propagate downwards into a layered half-space and as most inversion algorithms work with a one dimensional model, the subsurface is assumed to be homogeneous in the horizontal direction (Christiansen et al. 2006).

## 2.2 State of The Art

Even with these limitations the TEM method has found widespread application in environmental applications like groundwater explo-

ration (Danielsen et al. 2003; Sorensen et al. 2004; Auken et al. 2019), delineating saline intrusions into the groundwater (Gómez et al. 2019; Gonzales Amaya et al. 2018), characterising the subsurface below continental water bodies (Aigner et al. 2021), and the detection of karstic features (Zhou et al. 2022; Su et al. 2024).

### 2.2.1 Environmental Applications of TEM

Danielsen et al. (2003) used the TEM method for the exploration of buried valleys as potential aquifers in Denmark. The study introduced two new TEM systems based on the Geonics PROTEM: The high moment transient electromagnetic (HiTEM) system for a deeper investigation depth, and the pulled array Transient electromagnetic (PATEM) system for a higher lateral resolution. The HiTEM system uses a combination of a  $30 \times 30$  m transmitter loop and a current of 75 m to achieve a depth of investigation (DOI) of up to 300 m (Danielsen et al. 2003). To mitigate distortion effects a HiTEM sounding is split into two parts: A 70 m offset loop configuration for the later time data, and a central loop configuration with a reduced current of 2.5 A for the early times (Danielsen et al. 2003). A mutually constrained inversion (MCI) like in Auken et al. (2005) is used to invert the combination of the data gathered with the two different configurations (Danielsen et al. 2003). Danielsen et al. (2003) developed the PATEM system to use a  $3 \times 5$  m transmitter loop on a wheeled frame with an offset receiver loop, which allows for continuous measurements along a profile and a DOI of 100 – 150 m. To achieve a high DOI and useful near surface information, the PATEM system allows for a transmitter configuration with either 2 turns with 16 A or 8 turns with 40 – 50 A (Danielsen et al. 2003). That study also touches on the problems resulting from coupling with man-made structures. Coupling noise can be described as the noise introduced through induced currents in man-made structures, which changes the decay characteristics of the secondary magnetic field, and can be divided into galvanic and capacitive (Christiansen et al. 2006). Galvanic coupling is caused by grounded conductors like power lines and causes an underestimation of

the resistivity (Christiansen et al. 2006). Capacitive coupling is caused by current being generated in the conductor and leaking into the ground through an insulation, which leads to an oscillating signal (Christiansen et al. 2006). For this reason the Danielsen et al. (2003) recommend keeping a distance of about 150 m from underground cables or pipes when the earth has a resistivity of  $40 - 50 \Omega\text{m}$ .

Similarly to the PATEM system, Auken et al. (2019) propose a towed transient electromagnetic (tTEM) system for an efficient 3D mapping of the subsurface. The tTEM system utilises a  $2 \times 4$  m transmitter loop mounted on a non-conductive sled towed by a vehicle, which enables a production rate of about  $1 \text{ km}^2$  per day (Auken et al. 2019). The receiver loop is towed at 9 m offset from the transmitter (Auken et al. 2019). Like the PATEM system (Danielsen et al. 2003), the tTEM system (Auken et al. 2019) permits the use of two different currents (2.8 and 30 A) in order to gain a relatively high DOI of up to 70 m, while still allowing the investigation of shallow depths. Auken et al. (2019) also highlight the importance of considering the coupling effects of the system with conductive objects and it tests the system in an environment with a high resistivity of the subsurface ( $> 600 \Omega\text{m}$ ). Under these circumstances the signal caused by coupling can be observed in isolation and the study found that a minimal distance of 3 m between transmitter and vehicle was necessary to mitigate coupling effects (Auken et al. 2019).

Electromagnetic methods do not require direct contact with the subsurface, which allowed for the development of airborne electromagnetic methods (AEM) (Christiansen et al. 2006). Sorensen et al. (2004) introduced the SkyTEM system as an alternative to ground based TEM systems. The SkyTEM system uses a helicopter to carry a  $12.5 \times 12.5$  m transmitter loop with 4 turns and a receiver loop ( $0.5 \times 0.5$  m) in a central configuration (Sorensen et al. 2004). Just like the PATEM and HiTEM systems (Danielsen et al. 2003), a low moment and a high moment configuration are used to achieve a high DOI while still resolving the near surface layers (Sorensen et al. 2004). In the low moment configuration the current of 35 A only flows through one turn and for the high mo-

ment 50 A are used with all 4 turns (Sorensen et al. 2004). Sorensen et al. (2004) validated the SkyTEM system against a ground based TEM system with a transmitter loop size of  $40 \times 40$  m, showing a good agreement (below 5% deviation). This system is able to cover a larger area than traditional ground based systems in the same amount of time, while still being able to resolve underground structures, such as buried valleys (Sorensen et al. 2004).

**Revised until here** To investigate the subsurface below continental bodies of water, Aigner et al. (2021) propose a flexible single loop system which can be towed by a boat. By using a single loop which is kept afloat by several PVC pipe segments that keep it in a circular shape, the system can easily be moved around the lake. Using pipe segments allows for different loop sizes and thus different investigation depths. The TEM-FAST 48 system by Applied Electromagnetic Research (AEMR) was used to investigate the subsurface of the Lake Langau in Austria. A current of 4 A and loops with radii between  $6.2 - 11.9$  m were used, leading to an investigation depth between  $6.2 - 50.0$  m, which was sufficient to detect sedimentary layers below the lake. For a proper interpretation of early time data, it is important to understand how long the turn-off time of the transmitter for a single-loop setup is. When the transmitter is turned off, the current in the loop takes a certain amount of time to decay, which is called the turn-off ramp. This time was measured to be between  $4.2 - 10.4 \mu\text{s}$  – depending on loop size and resistivity of the subsurface. Using this information, a formula was derived to find the minimum effective sounding depth:

$$h_{\text{eff}} = \sqrt{t_{\text{eff}} \bar{\rho}} \quad (2)$$

where  $h_{\text{eff}}$  is the minimum effective sounding depth,  $t_{\text{eff}}$  is the minimum effective time and  $\bar{\rho}$  is the average resistivity of the smooth subsurface model. The study also showcased two different approaches to finding the DOI. The first uses different starting models for the inversion assuming that the DOI is reached when the data does not influence the inverted model

anymore and will keep the values of the starting model. The second approach is based on:

$$\text{DOI} \approx 0.55 \left( \frac{M \times \bar{\rho}}{\eta} \right) \quad (3)$$

where  $M$  is the magnetic moment,  $\bar{\rho}$  is the average resistivity of the smooth subsurface model and  $\eta$  is the noise level. Both methods agree on a DOI ranging between 20 and 50 m depending on the loop size.

As other water sources become less reliable in some regions in Bolivia, Gonzales Amaya et al. (2018) show the potential of the TEM method for the exploration of groundwater in the Punata alluvial fan. This aquifer is an important water source, but it has zones with high salinity, which poses challenges in its use. This study used the ABEM WalkTEM system with a  $50 \times 50$  m transmitter loop with a current of 18 A and two receiver loops ( $0.5 \times 0.5$  m and  $10 \times 10$  m) in a central configuration. This way a DOI of up to 200 m was achieved in some regions of the alluvial fan, while in other regions the DOI was limited to 80 m. The study was able to detect zones with high salinity and the results were validated with borehole data.

Gómez et al. (2019) conducted a similar study in the Challapampa area, Bolivia. In this study the same WalkTEM system and loop sizes were used as in the study by Gonzales Amaya et al. (2018). However, the receiver loops were deployed in an offset configuration and for the  $0.5 \times 0.5$  m loop only a current of 2 A was used, while the whole 18 A were applied for the  $10 \times 10$  m loop. This setup achieved a depth of investigation (DOI) of up to 250 m and identified the influence of a hot spring, which appeared as a low-resistivity zone, indicating higher salinity.

Another application of TEM is the detection of karstic features, like caves, faults, and fracture zones (Zhou et al. 2022; Su et al. 2024). Traditionally, a large transmitter loop size in the order of 100 m side length was used to achieve a high investigation depth. For this reason the TEM method was not suitable for the application in mountainous regions. However, a similar investigation depth can be achieved by using a smaller transmitter loop size and more turns. A multi-turn setup has the disadvantage of mu-

tual inductance caused by the large number of turns, which can lead to underestimation of the resistivity of the subsurface.

Zhou et al. (2022) proposed a coincident configuration with a  $2 \times 2$  m and 10 turns for the transmitter loop and 20 turns for the receiver loop. In order to mitigate the effects of the mutual inductance, borehole and electrical resistivity tomography (ERT) data were used to constrain the inversion. Because boreholes and ERT measurements are expensive and time-consuming, they are only used to correct the TEM soundings in order to account for shifted resistivity values. This method was used to detect a karst channel in Zhijin, China.

A more in-depth study on how to deal with self and mutual inductance was conducted by Su et al. (2024). Here a central loop configuration (receiver loop in the centre of the transmitter loop) was compared with a multi-turn small fixed-loop configuration (using multiple different receiver positions, while keeping the transmitter loop fixed). For the fixed-loop set up a correction coefficient was introduced to account for off-centre receiver positions. 5 model tests were conducted in order to compare the two configurations and the results showed that after correction the fixed-loop configuration was more accurate in detecting the position of one or multiple anomalies.

## 2.2.2 Common resistivity values

Electrical resistivity is a key parameter in geophysical investigations, as it provides valuable information about the properties of the Earth's subsurface. Many electrical and electromagnetic methods rely on constructing a model of the electrical resistivity distribution to characterise subsurface materials. By analysing these resistivity values, it is possible to infer the composition of subsurface layers and detect geological structures such as faults, fractures, and aquifers (Christiansen et al. 2006).

Table 1 presents commonly reported resistivity values for different subsurface materials. These values have been compiled from multiple studies conducted in diverse geological settings and using various geophysical methods (Gómez et al. 2019; Galazoulas et al. 2015; George et al. 2022).

**Tab. 1:** Common Resistivity Values of Sub-surface Materials

| Material                            | Resistivity ( $\Omega\text{m}$ ) |
|-------------------------------------|----------------------------------|
| Saturated layers with high salinity | 0.1 – 5                          |
| Saturated clays and silts           | 5 – 15                           |
| Saturated sediments                 | 10 – 20                          |
| Unsaturated sediments               | 50 – 80                          |
| Saturated sand                      | 40 – 150                         |
| Unsaturated sand                    | 400 – 1500                       |

In the context of Table 1, the term “sediments” refers to unconsolidated deposits consisting of a mixture of sand, silt, and clay. The precise resistivity values presented in Table 1 for sediments are not general global values but are specific to the study region investigated by Gómez et al. (2019). These values reflect the characteristics of sediments found in the Challapampa aquifer in Bolivia, where variations in grain size, moisture content, and mineral composition influence the resistivity measurements.

## 2.2.3 Data Inversion

A typical geophysical problem can be defined as follows:

$$\mathbf{d} = \mathcal{F}(\mathbf{m}) \quad (4)$$

where  $\mathbf{d}$  is the observed data,  $\mathcal{F}$  is the forward operator, and  $\mathbf{m}$  is the model. If the model is known, the forward operator can be used to calculate the expected data. Unfortunately, usually the model is unknown and the observed data is used to find the model, which is called an inverse problem. In practise the observed data is contaminated with noise, which introduces an error term into the equation and makes the inversion ill-posed and non-linear. An ill-posed problem means that small changes in the observed data can cause large differences in the model. As a result, noise introduces variability, making it impossible to find a unique solution (Zhdanov 2002).

Approaches to address this issue can be divided into deterministic and stochastic methods. The deterministic approach tries to find a single solution, by iteratively updating the model parameters to minimise the difference between observed and modeled data. To prevent overfitting to noise, Tikhonov regularisation is used,

which adds a penalty term to the least squares problem.

$$\|\mathbf{W}_d(\mathcal{F}(\mathbf{m}) - \mathbf{d})\|_2^2 + \lambda \|\mathbf{W}_m(\mathbf{m} - \mathbf{m}_0)\|_2^2 \rightarrow \min \quad (5)$$

$\mathbf{W}_d$  and  $\mathbf{W}_m$  are weighting matrices,  $\mathbf{m}_0$  is the initial model, and  $\lambda$  is the regularisation parameter.  $\|\mathbf{W}_m(\mathbf{m} - \mathbf{m}_0)\|_2^2$  can be interpreted as the roughness of the model, which quantifies the complexity or variation of the model.  $\|\mathbf{W}_d(\mathcal{F}(\mathbf{m}) - \mathbf{d})\|_2^2$  is the data misfit, which quantifies the difference between observed and modeled data and can include an error term. With the choice of  $\lambda$ , the trade-off between data misfit and model complexity can be controlled. Building on this foundation, several deterministic methods have been developed, such as Gauss-Newton inversion and Conjugate Gradient. A constraint inversion can be used to incorporate prior information about the model, which can be useful to prevent overfitting to noise. Stochastic methods, on the other hand, randomly search the solution space and provide a range of plausible models rather than a single deterministic solution. This is significantly more computationally expensive, but can be more robust against noise and can provide uncertainty estimates. Particle swarm optimization (PSO) and Bayesian inversion are examples of stochastic methods (Rücker et al. 2017; Xue et al. 2020).

An implementation of the deterministic approach is the PyGIMLi library, introduced by Rücker et al. (2017), which uses Gauss-Newton inversion to iteratively update the model parameters. PyGIMLi is an open-source library written in Python and C++ and is designed for the inversion of geophysical data. It allows the implementation of any given forward operator into the inversion algorithm, which makes it a versatile tool for geophysical modeling and inversion.

## 2.2.4 L-curve method

Solving inverse problems is a task not limited to geophysics, which makes inversion theory an important field in mathematics. There are several methods to solve an inverse problem, but the most common approach is to use Tikhonov

regularisation (5). But the choice of the regularisation parameter  $\lambda$  is not trivial and can have a significant impact on the inversion result.

The L-curve method is widely used to determine the optimal  $\lambda$  for the solution of an inverse problem (Hansen 1992). The L-curve is a graph of the residual norm against the solution norm. With an increasing  $\lambda$ , the residual norm is expected to increase and the solution norm is expected to decrease. This leads to a curve that resembles an L-shape. An optimal  $\lambda$  should minimise the residual norm while keeping the solution norm small. This leads to the “corner” of the L, which is also the point with the highest curvature.

Lloyd et al. (1997) implements a method to find the point of maximum curvature and through this the optimal  $\lambda$  for the inversion of diffusion battery data. The method computes the  $\chi^2$ , also called “error weighted root-mean-square”, and the roughness of the model for different  $\lambda$  values to obtain the L-curve. A cubic spline function is fitted to the data points, to make it possible to calculate the curvature for each data point:

$$\mathbf{C}(\lambda_i) = \frac{d^2 s / dx^2}{(1 + (ds/dx)^2)^{3/2}} \quad (6)$$

$$x = \log_{10} \chi^2(\lambda_i)$$

and find the point with the maximum curvature. The corresponding  $\lambda$  is then considered the optimal one. This method was not developed for geophysical data, but a model roughness and  $\chi^2$  can be computed for the TEM data as well.

A similar approach was used by Farquharson et al. (2004) to find the optimal  $\lambda$ . In this method the value of the regularization parameter  $\lambda$  is refined in each iteration of the data inversion. The inversion is started with a large  $\lambda$  and the L-curve is calculated. Then the curvature for the chosen  $\lambda$  is calculated through the formula:

$$\mathbf{C}(\lambda) = \frac{\zeta' \eta'' - \zeta'' \eta'}{[(\zeta')^2 + (\eta')^2]^{3/2}} \quad (7)$$

$$\zeta = \log \phi_d^{\text{lin}}$$

$$\eta = \log \phi_m$$

$\phi_d^{\text{lin}}$  is the data misfit and  $\phi_m$  is the model roughness. For the next iteration a new  $\lambda$  is calculated based on:

$$\lambda^n = \max(c\lambda^{n-1}, \lambda^{\max}) \quad (8)$$

where  $\lambda^n$  is the new  $\lambda$  value,  $\lambda^{n-1}$  is the previous  $\lambda$  value,  $0.01 \leq c \leq 0.5$  and  $\lambda^{\max}$  is the value for  $\lambda$ , which maximises the curvature. This cooling-schedule-type behaviour is added to prevent the inversion to skip to low values of  $\lambda$ , which is supposed to prevent artifacts created by overfitting the data. This method was tested on synthetic frequency domain electromagnetic data and was able to achieve an appropriate fit of inverted to the observed data.

Another approach for finding the optimal  $\lambda$  is the iterative golden section search as proposed by Cultrera et al. (2020). After providing an initial range for the optimal  $\lambda$   $[\lambda_1, \lambda_4]$ , two more  $\lambda$  values are calculated using the formula:

$$\begin{aligned} \varphi &= \frac{1 + \sqrt{5}}{2} \\ \lambda_2 &= 10^{\frac{\log_{10} \lambda_4 + \varphi \cdot \log_{10} \lambda_1}{1 + \varphi}} \\ \lambda_3 &= 10^{\log_{10} \lambda_1 + (\log_{10} \lambda_4 - \log_{10} \lambda_2)} \end{aligned} \quad (9)$$

For each  $\lambda$  the corresponding point on the L-curve is found and two curvatures ( $C_2$  and  $C_3$ ) are computed relying on three points each.  $C_2$  is the curvature of the points  $\lambda_1$ ,  $\lambda_2$ , and  $\lambda_3$ .  $C_3$  is the curvature of the points  $\lambda_2$ ,  $\lambda_3$ , and  $\lambda_4$ . Then  $\lambda_1$  or  $\lambda_4$  is omitted depending on which curvature is larger and a fourth  $\lambda$  is calculated based on the formula for  $\lambda_2$  (9). This process is repeated until the difference between the lambda-values of the interval are below a certain threshold. This method allows to find an optimal  $\lambda$  while minimising the number of inversions necessary. The search algorithm was tested with the ERT method on a conductive thin film with two non-conductive anomalies and showed promising results in finding the “corner” of the L-curve.

## 2.3 Experimental Set Up

In order to investigate the applicability of automatically determining an optimal lambda value to TEM data, we conducted a field survey in October of 2024 at the Martenhofer Lacke in the Nationalpark Neusiedlersee - Seewinkel. The

Geophysics Research Unit at TU Wien kindly provided data from May 2024 for the same location but with a differing measuring configuration, which enables a comparison between varying setups.

Furthermore a python package was developed to read, filter, and invert the TEM data. The visualisation of an L-curve as well as several methods of automatically finding an optimal lambda were also implemented.

### 2.3.1 Measuring Device

Both survey were conducted with the TEM-Fast 48 HPC system by Applied Electromagnetic Research (AEMR). It is compact device allowing the use of a single-loop configuration. By connecting an external 12 / 24 V battery a current either 1 / 4 A can be put through the connected transmitter loop. It records up to 48 logarithmically spaced time gates, which results in a time range between 4–16000  $\mu\text{s}$ . The specific number of time gates can be chosen through a time-key. Table 2 shows which time-key leads to which recording time range. To provide an optimal signal-to-noise ratio the device automatically stacks multiple pulses (Barsukov et al. 2006). The number of stacks are given by the formula  $P_{tot} = 13 \times n_s \times n_{as}$  (Aigner et al. 2021), where  $n_s$  (1–20) is the chosen stacking-key and  $n_{as}$  is the number of analogue stacks depending on the chosen time-key and can be found in Table 2. More detailed information on the device can be found in the manual provided on the website <http://www.aemr.net/tem-fast.htm>.

### 2.3.2 Field Survey

The field measurements were carried out at the Martenhofer Lacke in the *Nationalpark Neusiedlersee - Seewinkel* ( $16^\circ 51' 23.058''$  N,  $47^\circ 45' 8.4348''$  E), which is located on the east side of the Neusiedler See, Austria. Being part of the Seewinkel, which are intermittent alkaline soda waters, this water cycle of this lake is fueled by deep saline groundwater and evaporation leading to its high salinity and shallow water depth, which also varies throughout the year (Boros et al. 2025). This location was chosen due to having sparse man-made structures in the Nationalpark, which reduces noise in the gathered data to a minimum (Aigner et al. 2024).

**Tab. 2:** Parameters relating to the time-key of the TEM-FAST 48 HPC system (Excerpt from the manual).

| Key | Max Time ( $\mu\text{s}$ ) | Time Gates | Analogue Stacks |
|-----|----------------------------|------------|-----------------|
| 1   | 64                         | 16         | 1024            |
| 2   | 128                        | 20         | 512             |
| 3   | 256                        | 24         | 256             |
| 4   | 512                        | 28         | 128             |
| 5   | 1024                       | 32         | 64              |
| 6   | 2048                       | 36         | 32              |
| 7   | 4096                       | 40         | 16              |
| 8   | 8192                       | 44         | 8               |
| 9   | 16384                      | 48         | 4               |

The first survey, consisting of 45 soundings as shown in Figure 2 with a  $12.5 \times 12.5 \text{ m}$  loop, was carried out on the 22nd May 2024 and for the second survey 66 soundings, visualised in Figure 3 with a  $6.25 \times 6.25 \text{ m}$  loop were measured on 8th October 2024. For both surveys a voltage of 24 V was used and Table 3 shows the parameters for each sounding. Based upon a first visual inspection of the data some soundings were marked as "anomalous" as seen in Figures 2 and 3.

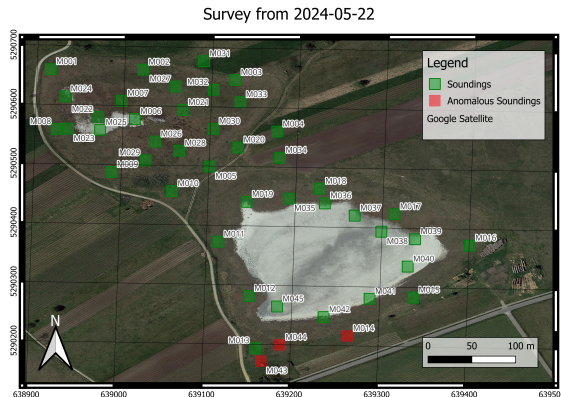


**Fig. 2:** Locations of all the TEM soundings measured in the first survey (22nd May 2024), where soundings are marked as anomalies, which fell out of order in a first visual inspection.

### 2.3.3 Python Package

In order to process the gathered data, we developed a python package mainly based on open-source python libraries. For the inversion routine we built upon the work of Aigner et al.

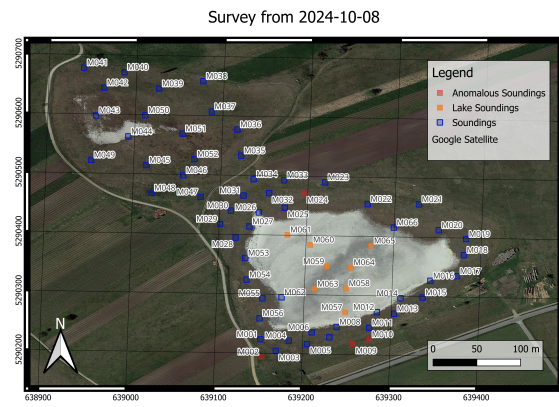


**Fig. 3:** Locations of all the TEM soundings measured in the second survey (8th October 2024), where soundings are marked as anomalies, which fell out of order in a first visual inspection.

(2021), which combines the electromagnetic wave modelling capabilities of `empymod` (Werthmüller 2017) with the inversion algorithm from `PyGIMLi` (Rücker et al. 2017).

The capabilities of this package include the reading of TEM data, adding coordinates to each sounding, the filtering based upon a time interval, and the visualisation of the raw with the filtered data. The inversion routine requires certain starting parameters like the lambda value, a layer distribution, a start model, and the relative error of the measured signal. If not specified otherwise a homogeneous model with the median apparent resistivity of the sounding is used as the starting model and the relative error is computed based of the error output of the measuring device. In case of particularly noisy

**Tab. 3:** Device settings used as well as the resulting measured time ranges and total number of pulses stacked for each sounding of both surveys.

| Sounding                | Current | Time Range      | Time Key | Stacking Key | Total Stacks |
|-------------------------|---------|-----------------|----------|--------------|--------------|
| <b>22nd May 2024</b>    |         |                 |          |              |              |
| M001, M002              | 4.1 A   | 4 – 480 $\mu$ s | 4        | 3            | 4992         |
| M003 – M014             | 1.0 A   | 4 – 480 $\mu$ s | 4        | 3            | 4992         |
| M015 – M045             | 1.0 A   | 4 – 240 $\mu$ s | 3        | 3            | 9984         |
| <b>8th October 2024</b> |         |                 |          |              |              |
| M001 – M066             | 4.1 A   | 4 – 240 $\mu$ s | 3        | 5            | 16640        |

data it is possible to set a minimum value for the relative error (noise floor). The noise floor limits how strongly the inversion algorithm tries to fit the model to each data point to avoid fitting errors. This inversion algorithm works with a model of the subsurface, where a resistivity value is assigned to a layer with a certain thickness, and only modifies the resistivity value of every layer while keeping the thicknesses fixed. This makes the choice of an appropriate layer distribution (specifying the number and thicknesses of layers) vital (Welkens 2025).

We also implemented the functionality to compute and visualise an L-Curve for a TEM sounding. For this we run the inversion for various logarithmically spaced lambda values, specified by the lower bound, the upper bound, and the number of values. For each inversion, we compute the root-mean-square (RMS) misfit of the data with the model as well as the roughness of the model and use these two values as the coordinates of a point corresponding to each inversion, which should result in an L-Curve (Cultrera et al. 2020; Hansen 1992).

To find an optimal lambda value for the inversion we implemented several search algorithms, which all try to find the point (corresponding to a lambda value) with the highest curvature on the L-Curve (Lloyd et al. 1997; Cultrera et al. 2020). We implemented the method used by Lloyd et al. (1997), which fits a cubic spline function to the L-Curve and computes the first and second derivative of this function, which are used to compute the curvature of the function at each point. We also implemented a similar approach, where we used the `numpy.gradient` function (<https://numpy.org/doc/1.26/reference/generated/numpy.gradient.html>) to com-

pute the first and second derivative for the curvature. Lastly we implemented the iterative golden section search algorithm as described by Cultrera et al. (2020), where a lower and upper bound is defined for the lambda value and by comparing two curvatures within the interval and discarding the lower one, this method contracts the interval towards the optimal lambda. The advantage compared to the other two methods is that it is not bound to the predefined list of logarithmically spaced lambda values, which in theory allows a more precise determination of the optimal lambda.

### 3 Results

### 4 Conclusion

### List of Figures

|   |  |   |
|---|--|---|
| 1 | Numerically modelled typical TEM response with the used subsurface model (a), the signal (b), and the apparent resistivity (c) . . . . . | 2 |
| 2 | Map of Sounding Locations in May . . . . .   | 8 |
| 3 | Map of Sounding Locations in October . . . . .   | 8 |

### List of Tables

|   |   |   |
|---|---|---|
| 1 | Common Resistivity Values of Subsurface Materials . . . . . | 5 |
| 2 | Time Key Parameters of the TEM-FAST Device . . . . .        | 8 |
| 3 | Device Settings in Both Surveys . . . . .                   | 9 |

## Declaration of competing interest

The authors declare that they have no known competing financial interests or personal relationships that could have appeared to influence the work reported in this thesis.

## Data availability

The python package for this thesis was developed in cooperation with Welkens (2025) and is building upon the routine from Aigner et al. (2021). It is available open-source and can be accessed on github ([https://github.com/pb-tuwien/Bsc\\_TEM\\_tools.git](https://github.com/pb-tuwien/Bsc_TEM_tools.git)). To facilitate full reproducibility of the results all data and python routines used throughout this work can also be accessed on github ([https://github.com/pb-tuwien/BSc\\_Soda\\_Lakes\\_Balogh.git](https://github.com/pb-tuwien/BSc_Soda_Lakes_Balogh.git))

## References

- Aigner, L., P. Högenauer, M. Bücker, and A. Flores Orozco (2021). “A Flexible Single Loop Setup for Water-Borne Transient Electromagnetic Sounding Applications”. In: *Sensors* 21.19, pp. 6624–. DOI: [10.3390/s21196624](https://doi.org/10.3390/s21196624).
- Aigner, L., D. Werthmüller, and A. Flores Orozco (Apr. 1, 2024). “Sensitivity analysis of inverted model parameters from transient electromagnetic measurements affected by induced polarization effects”. In: *Journal of Applied Geophysics* 223, p. 105334. DOI: [10.1016/j.jappgeo.2024.105334](https://doi.org/10.1016/j.jappgeo.2024.105334).
- Auken, E., N. Foged, J. J. Larsen, K. V. T. Lassen, P. K. Maurya, S. M. Dath, and T. T. Eiskjær (Jan. 2019). “tTEM — A towed transient electromagnetic system for detailed 3D imaging of the top 70 m of the subsurface”. In: *GEOPHYSICS* 84.1, E13–E22. DOI: [10.1190/geo2018-0355.1](https://doi.org/10.1190/geo2018-0355.1).
- Auken, E., L. Pellerin, and K. I. Sørensen (2005). “Mutually constrained inversion (MCI) of electrical and electromagnetic data”. In: *SEG Technical Program Expanded Abstracts 2001*, pp. 1455–1458. DOI: [10.1190/1.1816378](https://doi.org/10.1190/1.1816378).
- Barsukov, P., E. Fainberg, and E. Khabensky (Jan. 1, 2006). “Chapter 3 Shallow Investigations by TEM-FAST Technique: Methodology and Examples”. In: *Methods in Geochemistry and Geophysics*. Ed. by V. V. Spichak. Vol. 40. Elsevier, pp. 55–77. ISBN: 0076-6895. DOI: [10.1016/S0076-6895\(06\)40003-2](https://doi.org/10.1016/S0076-6895(06)40003-2).
- Boros, E. and L. Vörös (2025). “How Can Unique Alkaline Soda Waters Be Managed and Restored? Lake Neusiedl as the Largest Threatened European Example”. In: *Ecohydrology* 18.2, e2738. DOI: [10.1002/eco.2738](https://doi.org/10.1002/eco.2738).
- Chandra, P. C. (2016). “The time domain electromagnetic method”. In: *Groundwater Geophysics in Hard Rock*. Milton, UNITED KINGDOM: Taylor & Francis Group, pp. 233–261. ISBN: 978-0-203-09367-2.
- Christiansen, A. V., E. Auken, and K. Sørensen (2006). “The transient electromagnetic method”. In: *Groundwater Geophysics: A Tool for Hydrogeology*. Ed. by R. Kirsch. Berlin, Heidelberg: Springer Berlin Heidelberg, pp. 179–225. ISBN: 978-3-540-29387-3. DOI: [10.1007/3-540-29387-6\\_6](https://doi.org/10.1007/3-540-29387-6_6).
- Cutrera, A. and L. Callegaro (Aug. 2020). “A simple algorithm to find the L-curve corner in the regularisation of ill-posed inverse problems”. In: *IOP SciNotes* 1.2, p. 025004. DOI: [10.1088/2633-1357/abad0d](https://doi.org/10.1088/2633-1357/abad0d).
- Danielsen, J. E., E. Auken, F. Jørgensen, V. Søndergaard, and K. I. Sørensen (Oct. 1, 2003). “The application of the transient electromagnetic method in hydrogeophysical surveys”. In: *Journal of Applied Geophysics*. Geophysical Investigations of Buried Quaternary Valleys in the Formerly Glaciated NW European Lowland: Significance for Groundwater Exploration 53.4, pp. 181–198. DOI: [10.1016/j.jappgeo.2003.08.004](https://doi.org/10.1016/j.jappgeo.2003.08.004).
- Everett, M. E. (2013). “Electromagnetic induction”. In: *Near-Surface Applied Geophysics*. United States: Cambridge University Press, pp. 200–238. ISBN: 978-1-107-01877-8.
- Farquharson, C. G. and D. W. Oldenburg (2004). “A comparison of automatic techniques for estimating the regularization parameter in non-linear inverse problems”. In: *Geophysical Journal International* 156.3, pp. 411–425. DOI: [10.1111/j.1365-246X.2004.02190.x](https://doi.org/10.1111/j.1365-246X.2004.02190.x).

- Fitterman, D. V. and M. T. Stewart (1986). “Transient electromagnetic sounding for groundwater”. In: *Geophysics* 51.4, pp. 995–1005. DOI: 10.1190/1.1442158.
- Galazoulas, E. C., Y. C. Mertzanides, C. P. Petalas, and E. K. Kargiotis (Mar. 1, 2015). “Large Scale Electrical Resistivity Tomography Survey Correlated to Hydrogeological Data for Mapping Groundwater Salinization: A Case Study from a Multilayered Coastal Aquifer in Rhodope, Northeastern Greece”. In: *Environmental Processes* 2.1, pp. 19–35. DOI: 10.1007/s40710-015-0061-y.
- George, N. J., A. M. Ekanem, J. E. Thomas, and T. A. Harry (Mar. 1, 2022). “Modelling the effect of geo-matrix conduction on the bulk and pore water resistivity in hydrogeological sedimentary beddings”. In: *Modeling Earth Systems and Environment* 8.1, pp. 1335–1349. DOI: 10.1007/s40808-021-01161-0.
- Gómez, E., M. Larsson, T. Dahlin, G. Barmen, and J.-E. Rosberg (Jan. 28, 2019). “Alluvial aquifer thickness and bedrock structure delineation by electromagnetic methods in the highlands of Bolivia”. In: *Environmental Earth Sciences* 78.3, p. 84. DOI: 10.1007/s12665-019-8074-x.
- Gonzales Amaya, A., J. Mårdh, and T. Dahlin (Jan. 19, 2018). “Delimiting a saline water zone in Quaternary fluvial-alluvial deposits using transient electromagnetic: a case study in Punata, Bolivia”. In: *Environmental Earth Sciences* 77.2, p. 46. DOI: 10.1007/s12665-017-7213-5.
- Hansen, P. C. (1992). “Analysis of Discrete Ill-Posed Problems by Means of the L-Curve”. In: *SIAM review* 34.4, pp. 561–580. DOI: 10.1137/1034115.
- Lloyd, J. J., C. J. Taylor, R. S. Lawson, and R. A. Shields (Oct. 1, 1997). “The use of the L-curve method in the inversion of diffusion battery data”. In: *Journal of Aerosol Science* 28.7, pp. 1251–1264. DOI: 10.1016/S0021-8502(97)00018-9.
- Obukhov, G. (1968). “The Fields of a Horizontal Electric Dipole Over an Uneven Insulating Basement”. In: *Exploration Geophysics* 50, p. 100.
- Rücker, C., T. Günther, and F. M. Wagner (Dec. 1, 2017). “pyGIMLi: An open-source library for modelling and inversion in geophysics”. In: *Computers & Geosciences* 109, pp. 106–123. DOI: 10.1016/j.cageo.2017.07.011.
- Siemon, B. (2009). “Electromagnetic methods – frequency domain”. In: *Groundwater Geophysics: A Tool for Hydrogeology*. Ed. by R. Kirsch. Berlin, Heidelberg: Springer Berlin Heidelberg, pp. 155–178. ISBN: 978-3-540-88405-7. DOI: 10.1007/978-3-540-88405-7\_5.
- Sorensen, K. I. and E. Auken (Sept. 1, 2004). “SkyTEM—a New High-resolution Helicopter Transient Electromagnetic System”. In: *Exploration Geophysics* 35.3, pp. 194–202. DOI: 10.1071/EG04194.
- Su, M., M. Chu, Y. Xue, X. Ma, and Z. Ju (June 1, 2024). “Response analysis and application of the TEM using small-fixed loops”. In: *Acta Geotechnica* 19.6, pp. 3537–3553. DOI: 10.1007/s11440-023-02103-z.
- Welkens, J. (2025). “Comparison of subsurface geophysical models of Hutweidenlacke (Nationalpark Seewinkel) based on the Transient Electromagnetic Method”. Bachelor’s Thesis, unpublished. Vienna, Austria: Research Unit Geophysics, Department of Geodesy and Geoinformation, TU Wien.
- Werthmüller, D. (Nov. 2017). “An open-source full 3D electromagnetic modeler for 1D VTI media in Python: empymod”. In: *GEO-PHYSICS* 82.6, WB9–WB19. DOI: 10.1190/geo2016-0626.1.
- Xue, G., H. Li, Y. He, J. Xue, and X. Wu (2020). “Development of the Inversion Method for Transient Electromagnetic Data”. In: *IEEE Access* 8, pp. 146172–146181. DOI: 10.1109/ACCESS.2020.3013626.
- Zhdanov, M. S. (2002). *Geophysical Inverse Theory and Regularization Problems*. 1st ed. Methods in geochemistry and geophysics. Amsterdam: Elsevier. ISBN: 978-0-444-51089-1.
- Zhou, Y., P. Jianwei, L. Hao, W. Zhongmei, Z. Jiang, L. Haixin, and L. Jiaxu (Nov. 10, 2022). “Multi-turn small-loop transient electromagnetic data processing using constraints from borehole and electrical resistivity tomography data”. In: *Arabian Journal of Geosciences* 15.22, p. 1675. DOI: 10.1007/s12517-022-10952-3.